Experimental Study of Transient Waves in a Plane Grid Structure

William L. Hallauer Jr.* and Dinesh J. Trivedi†
Virginia Polytechnic Institute and State University, Blacksburg, Virginia

Flexural waves were generated and measured in a two-dimensional laboratory structure that is in many respects dynamically representative of flexible, large spacecraft structures. The structure's first vibration mode is at 0.6 Hz, and its average modal density for 0–100 Hz is 0.55 mode/Hz. The excitation used was suddenly applied sinusoidal forcing at a point on the structure, with frequencies from 15–240 Hz. Time-series motion responses were measured at several points on the structure, permitting observation of waves traveling outward from the point of excitation. Complementary theoretical transient responses were computed for a refined finite-element model of the laboratory structure, and the theoretical predictions are compared with the experimental measurements.

I. Introduction

STRUCTURAL wave propagation is a subject of current interest relative to the dynamics and control of flexible large spacecraft structures (LSS). Accordingly, theoretical studies of traveling waves in complex structures have been conducted recently, e.g., Refs. 1 and 2. However, there has been very little parallel experimental research. Several experiments on flexural waves in straight and uniform beams have been reported, beginning many years ago, e.g., Ref. 3, and continuing to the present, e.g., Ref. 4. But the only comparable research on waves in two- or three-dimensional framed structures known to the authors is the recent work of Williams et al.[5,6]

Despite the dearth of literature, experimental study of traveling waves in structures representative of LSS is clearly desirable to validate theoretical analysis methods. This paper reports such a study, the specific subject being flexural waves in a moderately complex plane grid composed primarily of thin-walled beams. This small laboratory structure is very flexible in out-of-plane bending. This flexibility is intended to represent in a generic sense that of an LSS, at least with respect to waves whose lengths are short relative to global structural dimensions but long relative to the thicknesses of beam members.

Although the primary focus of this paper is experimental analysis of transient waves, theoretical results complementary to the experiment are also presented. The theoretical procedure is standard, based on a refined finite-element linear model of the laboratory structure and integration of the full set of differential equations of motion describing the model.

A well-designed finite-element model is probably the best type of theoretical model available, in general, for predicting global response of a complex structure. However, the frequencies of traveling waves are usually above a structure's lowest natural frequencies, and even a highly-refined model often fails to predict accurately the modes beyond a few of the lowest. So the ability of a finite-element model to predict transient wave response is uncertain, and this ability is evaluated herein for the particular structure and finite-element model considered.

II. Excitation and Response Quantities for Transient Waves

The type of excitation used in this study is force applied at a point and having a suddenly applied sinusoidal (SAS) variation with time: $u(t)\sin\Omega t$, where $u(t)$ is the unit step at time $t=0$ and Ω is radian frequency. Although impact excitation has been used in most previous experimental studies of transient waves in beams, SAS excitation was preferred in this study for two reasons.

First, one objective of this work has been to evaluate the validity of theoretical analysis of transient waves by the finite-element method. It is well-known that the accuracy of vibration modes calculated for a finite-element model deteriorates progressively as mode number and natural frequency increase. Hence, it might be expected that the accuracy of calculated transient response would also deteriorate progressively as the predominant frequencies of response increase. SAS excitation has only one predominant frequency, i.e., Ω, so it is especially suitable for determining the variation of theoretical accuracy with frequency. A particularly relevant quantity is the range of SAS excitation frequencies, if any, over which the finite-element model predicts the measured transient response with reasonable accuracy.

Second, it seemed possible initially that SAS point-force excitation might permit the measurement of group and phase velocities in the dispersive laboratory structure, just as a similar type of excitation can in a beam. Bozich[7] showed that SAS displacement imposed on the edge of a semi-infinite beam produces a flexural displacement "wavefront" traveling at the group velocity into the beam's interior; the wavefront is preceded by low-level, high-frequency precursor waves and followed by higher-level synchronous waves, i.e., waves with the frequency of the sinusoidal excitation and traveling at the phase velocity.

Instrumentation developed previously in our laboratory is capable of producing an excitation time history closely approximating a true SAS force. The principal components are noncontacting force actuators and controlled-current power amplifiers,[8] the combination of which can accurately generate varying forces of very small magnitude on even an

Presented as Paper 87-0943 at the AIAA Dynamics Specialists Conference, Monterey, CA, April 9–10, 1987; received March 30, 1987; revision received June 12, 1987.

*Professor, Department of Aerospace and Ocean Engineering. Member AIAA.

†Graduate Research Assistant, Department of Aerospace and Ocean Engineering. Student Member AIAA.

extremely flexible, moving structure. In the absence of such instrumentation, the impact excitation forces used for most previous traveling wave experiments could not be tailored to have simple mathematical forms.

The transient wave response variables measured in this study are translational motion quantities: displacement, velocity, and acceleration. In contrast, most previous flexural wave experiments have used only strain gages and have inferred dynamic bending moments. Measurement of strains was consistent with the traditional practical motivation for studying structural waves: failure due to fracture or plastic deformation resulting from impact loading. However, measurement of motion quantities in this study was appropriate in the context of LSS dynamics and control. Future LSS in normal orbital operation will experience only mild environmental loading[9] and should be in little danger of structural failure. But control of motion caused by low-level disturbances will be necessary to satisfy operational requirements such as antenna pointing accuracy, and this control is likely to involve direct sensing of motions.

III. Pendulous Plane Grid Structure

The laboratory structure is illustrated in Fig. 1. The major components are a lightweight skewed grid of aluminum beams, two nominally identical thick aluminum plates, and a steel top beam assembly from which the grid and plates hang vertically. Mounting of the beam assembly in low-friction bearings produces a pendulum mode, the very low frequency of which is governed primarily by eccentricity Y of the plates. All members of the structure are bolted tightly together at joints, 12 of which are labeled on Fig. 1.

The structure has both out-of-plane and in-plane vibrational modes relative to the grid's plane, but the two types of modes are decoupled by the geometry. Only out-of-plane excitation and response are considered herein, so all subsequent discussion refers to out-of-plane dynamics.

The laboratory structure was designed to possess some of the important generic dynamic characteristics of LSS, in particular, many low-frequency vibrational modes, including some pairs of closely coupled modes. It has been used previously for studies of active vibration damping.[8,10] Several minor modifications have been made to the structure recently, so the specific modal data published previously do not apply to the present structure. However, the structure's general dynamic characteristics remain unchanged.

The skewed aluminum grid is extremely flexible, and it extends over an area of 2.4 m^2. These features would seem to qualify the grid as appropriate for an experimental study of two-dimensional traveling flexural waves. However, the grid's suitability was contingent on whether the available instrumentation was capable of measuring the waves. Preliminary hand calculations based on Euler-Bernoulli beam flexural wave speeds suggested that wave travel times between distant points of the grid would be on the order of several centiseconds for excitations with frequencies under 1 kHz. (The group velocity in a uniform beam is twice the phase velocity, which is $\sqrt[4]{(EI\Omega^2/\rho A)}$, where EI and ρA are bending stiffness and mass per unit length, respectively.) The decision was made to use the grid for this study because the hand-calculated values are indeed within the capabilities of the exciters, sensors, and the system for data acquisition and analysis available from earlier active vibration damping experiments.

Out-of-plane vibrational modes of the laboratory structure have been calculated theoretically and measured experimentally. A summary of the theoretical model and modal surveys is presented next.

The structure is modeled theoretically as an assemblage of 51 beam finite elements connected at 43 grid points, as shown in Fig. 2. The degrees of freedom (DOF) at each grid point are out-of-plane translation and rotations about the horizontal and vertical in-plane axes. Translations are restrained at grid points 34 and 43, so the total number of DOFs is 127.

The beam element structural stiffness and consistent mass matrices used for the aluminum grid are standard, with bending deformation based on Euler-Bernoulli theory and cubic shape functions, and torsional deformation based on elementary theory and linear shape functions.[11] Timoshenko theory would be required if bending wavelengths were on the order of beam thickness and frequencies were correspondingly high. But Euler-Bernoulli theory is quite satisfactory in this case, because the measurable oscillatory response consisted of waves with lengths at least two orders of magnitude greater than beam thickness, and excitation frequencies were 240 Hz or lower. Moreover, SAS excitation of frequency Ω, despite being impulsive, does not excite response at substantially higher frequencies; the Fourier transform of an SAS function peaks sharply at Ω but decays steeply with increasing frequency above Ω.

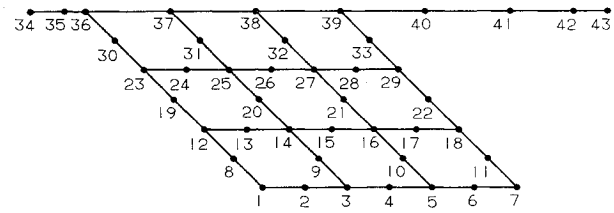

Fig. 2 Grid points (labeled) and beam elements of the 127-DOF finite-element model.

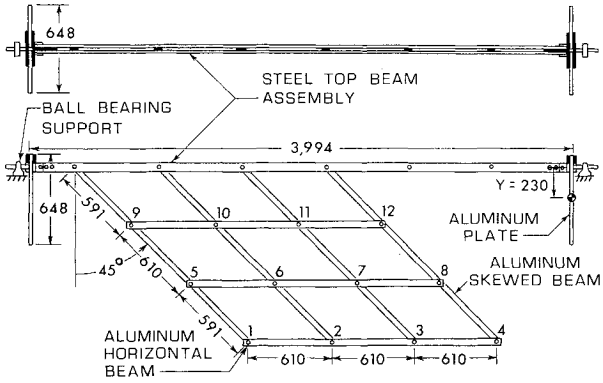

Fig. 1 Drawing of the laboratory structure, with dimensions in mm. Labels identify bolted joints of the aluminum grid. Nominal cross-sectional dimensions: steel beams, 63.5×12.7 mm; aluminum horizontal beams, 50.8×3.175 mm; aluminum skewed beams, 38.1×3.175 mm. Thickness of aluminum plates, 17.5 mm.

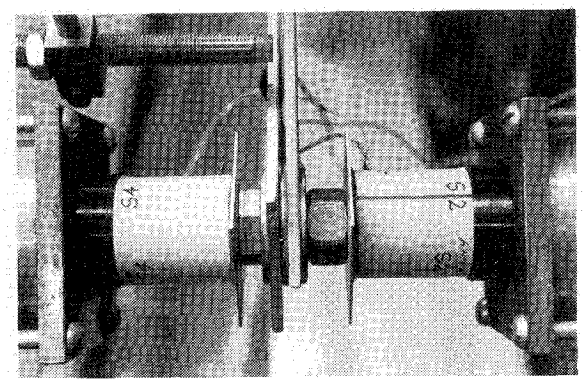

Fig. 3 Bolted joint 4, photographed from the right and above joint 4 in Fig. 1; displacement sensor (upper left), force actuator (lower left), and velocity sensor (right).

Gravity-induced in-plane axial forces, shear forces, and bending moments have significant influence on the out-of-plane stiffness of the thin-walled aluminum grid members. This influence is represented by element geometric stiffness matrices.[12]

The beam element stiffness and mass matrices of the steel top beam assembly are standard, with one exception: bending shear flexibility[13] is included to account at least roughly for the discontinuous sandwich design evident in the top view of Fig. 1.

The thick aluminum plates are modeled as rigid. The product of weight W times eccentricity Y of each plate acts as a pendulous rotational stiffness about the beam assembly axis at the location where the plate joins the beam assembly. This is modeled by the attachment of a grounded rotational spring with stiffness WY at each of the grid points 34 and 43.

Waves traveling in the aluminum grid encounter discontinuities due both to its spatially discontinuous geometry and to the concentrated inertia and local stiffening at each bolted joint. Figure 3 shows a typical joint. The inertias and local stiffening effects of handware at all joints of the laboratory structure are included in the finite-element model.

The stiffness and mass matrices of the complete model shown in Fig. 2 were assembled in the standard fashion of the matrix stiffness method, and they were used for calculation of all 127 vibrational modes of the model. This complete modal solution was used for calculation of transient response, as described in Sec. V.

Out-of-plane natural frequencies of the laboratory structure in the 0-100 Hz band were identified experimentally. Slow sine-sweep testing with single-point excitation[14] was the principal method used.

Figure 4 is a comparison of experimental and theoretical mode counts in the 0-100 Hz band. The finite-element model is clearly very good for the lowest 15 modes. The first difference detectable in Fig. 4 between theory and experiment is for mode 16, which is the second bending mode of the steel top beam assembly. This difference is indicative of relatively poor modeling of the beam assembly's discontinuous sandwich design. Although there are many other differences between individual modal frequencies in the 0-57 Hz band encompassing 39 modes, the theoretically predicted modal density is quite good in this band. For frequencies above 63 Hz, the finite-element model underestimates the modal density, and the prediction deteriorates progressively as frequency increases.

IV. Experimental Apparatus, Procedure, and Results

For most of the cases discussed in this paper, SAS force excitation was applied at joint 4 of the aluminum grid. Joint 4 was chosen to maximize the structural pathlength in the grid between the point of excitation and the most distant point of response measurement, joint 9 in this case. Motion sensors were positioned at all of the bolted joints to permit detection of the wavefront's progression leftward and upward through the grid.

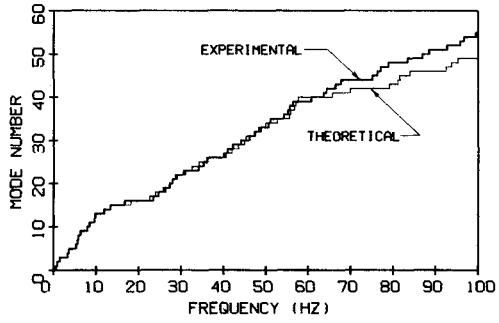

Fig. 4 Mode count diagram for the laboratory structure.

Selection of the SAS excitation frequencies used was based loosely on expected wavelengths and the comparison between experimental and theoretical mode counts in Fig. 4. In the context of expected LSS dynamics, it seemed appropriate that wavelengths should be short relative to global structural dimensions, say, no longer than about 0.9 m, which is half the length of each straight side of the aluminum grid. Equating 0.9 m with $2\pi\sqrt[4]{EI/\rho A\Omega^2}$), the length of a synchronous flexural wave in a uniform beam, gives the corresponding frequency $\Omega/2\pi$ to be about 30 Hz. Figure 4 shows that 30 Hz is within the band in which the theoretical model is accurate, at least for mode count and modal density. To permit more complete evaluation of the finite-element model's accuracy, frequencies both lower and higher than 30 Hz were used as well.

The experimental procedure for exciting and measuring transient response evolved through several stages of refinement. To assist in describing the experiments, we present next some sample measurements from the penultimate stage. The following 16 channels of time-series data were acquired: the signal proportional to excitation force on joint 4, signals from displacement sensors near joints 4 and 5, signals from velocity sensors at joints 1-12, and the signal from an accelerometer near joint 5. These signals were conditioned only by instrumentation gains and analog low-pass filters. Numerical postprocessing consisted only of multiplication by calibration factors and addition of constant time series to compensate for instrumentation DC offsets.

Data measured at joints 4 and 5 are shown in Fig. 5. The SAS force imposed on joint 4 begins at time $t=0$ s and has frequency $\Omega/2\pi=30$ Hz. Joint 4 responds immediately, and joint 5 begins to move after 0.03-0.04 s, the travel time between joints 4 and 5. The force magnitude in this and all tests was kept very low so that the structure, the force actuator, and the motion sensors would all operate linearly.

One tends to expect that response to SAS excitation will be primarily oscillatory at the SAS frequency. Hence, it may be surprising to observe displacement time series for joints 4 and 5, $D_4(t)$ and $D_5(t)$ in Fig. 5, in which the synchronous

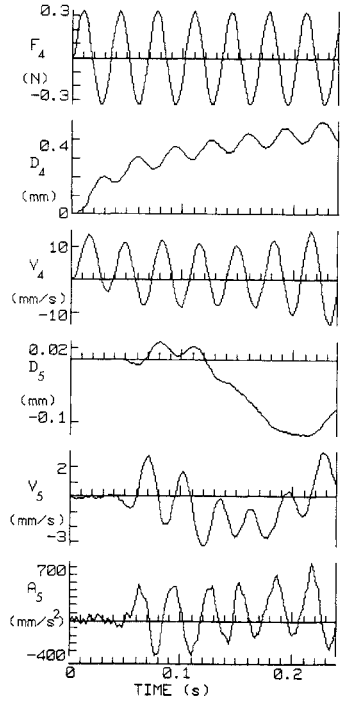

Fig. 5 Representative experimental results for 30-Hz SAS force at joint 4. Force, displacement, velocity, and acceleration are denoted by F, D, V, and A, respectively, and the subscript denotes joint number.

oscillatory components are subordinate to displacement components appearing to have much lower frequencies.

This observation motivated a theoretical analysis of a qualitatively similar but mathematically simpler problem, a single semi-infinite, uniform, Euler-Bernoulli beam under SAS force excitation at its edge.[15] The closed-form solution is similar to the displacement results in Fig. 5. In particular, the displacement of the excited edge of the semi-infinite beam for times after about one cycle of excitation, $t > 2\pi/\Omega$, is proportional to $2\sqrt{(\Omega t/\pi)} + \sin(\Omega t - 3\pi/4)$. Very similar to this solution is $D_4(t)$ in Fig. 5.

Unlike displacement of a semi-infinite beam, that of the grid does not increase indefinitely as the square root of time. Traveling waves reflect off the structure's finite boundaries and combine, and eventually the motion consists of periodic standing waves of finite amplitude. If the displacement time series of Fig. 5 were extended over a few seconds, they would display bounded oscillations about zero with dominant low-frequency components. Moreover, if the excitation is sustained for about half a minute, the small inherent damping of the structure suppresses all nonsynchronous components of response, and steady-state oscillatory response at frequency Ω is established.

As is explained in Sec. II, one reason for selection of SAS excitation was its potential to permit measurement of phase and group velocities in the grid. However, this objective could not be achieved with the motion-sensing instrumentation used, as is demonstrated by analysis of the joint 5 response in Fig. 5. It is difficult to infer from the joint 5 plots the time of arrival of the initial precursor wave, and it is probably impossible to identify a group velocity wavefront between precursor waves and synchronous waves.

One might expect that these quantities could be detected most clearly from the acceleration signal, since it should be most sensitive to high-frequency precursor waves and least sensitive to low-frequency nonsynchronous oscillations. But high-frequency sensitivity in this case is also noise sensitivity, and noise obviously obscures the times of precursor wave arrival and transition to synchronous waves on $A_5(t)$ of Fig. 5.

To avoid adding significant mass to the structure, it was necessary to use a 2-gram accelerometer. This device has nominal sensitivity of 10 mV/g, which is very low but typical for miniature accelerometers. Consequently, the accelerometer output signal magnitude that produced the $A_5(t)$ plot was only about one millivolt peak-to-peak, such a low signal level as to be very susceptible to noise.

The standard remedy for high-frequency electrical instrumentation noise is low-pass filtering, but this remedy should be applied very carefully, if at all, in measurement of transient waves. Butterworth 8-pole low-pass filters with 200-Hz corner frequency were used for the data of Fig. 5. An attempt to reduce noise by lowering the corner frequency below 200 Hz proved unsuccessful because the filters then produced unacceptable distortion of signal components at the excitation frequency. It was finally decided that minimizing distortion should have priority over minimizing noise. Hence, for all subsequent testing, the filter corner frequency of every data channel was set at 1000 Hz, the highest possible for the data acquisition system.

It is clear from Fig. 5 that the displacement and velocity signals were much stronger than the acceleration signal. Velocities were considered to be the best of the three types of measurement. Velocity signals had relatively low noise, permitting reasonably clear identification of wavefront arrival times, and they were not dominated by low-frequency components, as were the displacement signals, so they clearly displayed the synchronous oscillations in most cases. Consequently, only velocity response is considered in the remainder of this paper.

The excitation signal that produced force $F_4(t)$ of Fig. 5 was computed digitally and converted into a continuous voltage by a digital-to-analog converter (D/A). The D/A output signal has the stairstep character shown in the upper portion of Fig. 6. It was sent directly into a power amplifier,[8] which caused an electric current proportional to the D/A output voltage to flow through a coil attached to joint 4 (Fig. 3). The current interacted with a magnetic field to produce an out-of-plane force on joint 4 proportional to the current and therefore having the same stairstep character as the D/A output signal.

The coil current was sensed (as the voltage drop across a 1-ohm resistor in series with the coil) and multiplied by a

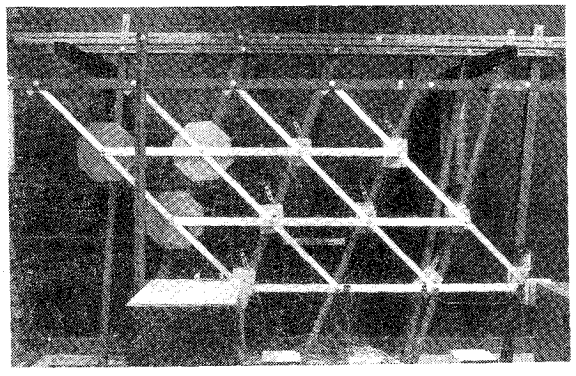

Fig. 7 Photograph of aluminum grid hanging from steel top beam assembly, and the surrounding framework.

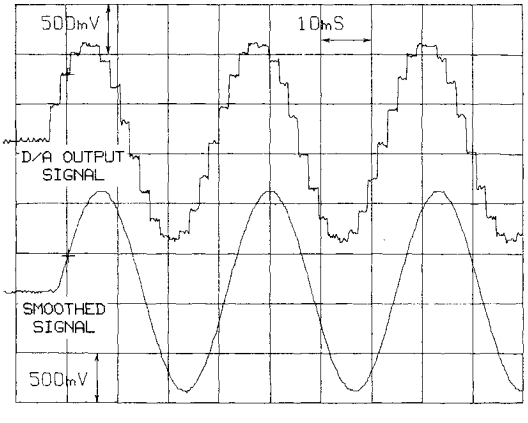

Fig. 6 30-Hz SAS D/A output voltage and smoothed voltage produced by linear-phase low-pass filtering, recorded from the screen of a digital oscilloscope.

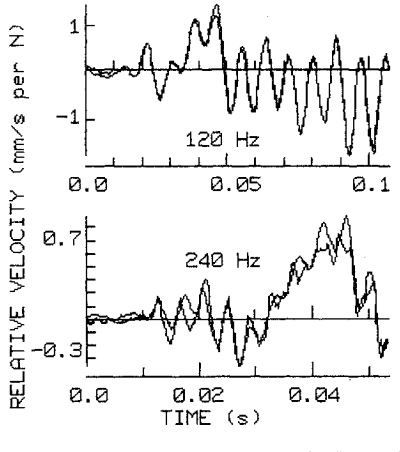

Fig. 8 Dynamic reciprocity measurements. Each graph consists of two time series: response at joint 1 due to SAS force at joint 4, and response at joint 4 due to SAS force at joint 1.

calibration factor to produce the $F_4(t)$ plot of Fig. 5. This plot does not accurately represent the actual stairstep character of the force, as shown in the upper portion of Fig. 6, because the dot-matrix plotter connects time-series data points with nominally straight lines.

Many refinements in experimental procedure and apparatus were made following the experiment that produced Fig. 5. One was smoothing of the D/A output signal so that the excitation force would have the character shown in the lower portion of Fig. 6, which is obviously a much better approximation to a true SAS curve than is the D/A output signal. The smoothed signal was produced by passing the D/A output signal through a Multimetrics Model AF-420L Active Filter, which was set to provide 8-pole, low-pass, linear-phase filtering. Transient wave tests were conducted for SAS excitation frequencies 15, 30, 45, 60, 90, 120, 150, and 240 Hz. For each frequency, the D/A rate used was $256[(\Omega/2\pi)/15]$ steps per second, and the smoothing filter corner frequency was set equal to the D/A rate.

The displacement sensors that produced $D_4(t)$ and $D_5(t)$ of Fig. 5 are Bently Nevada Corp. Type 300 noncontacting proximity probes with nominal sensitivity of 100 V/in. and linear range of about ± 1 mm for a steel target (Fig. 3). The piezoelectric accelerometer that produced $A_5(t)$ is a PCB Piezotronics Inc. Model 303A03.

The force actuators and velocity sensors are simple magnet-coil devices. Each type consists of a coil attached to a grid joint and an externally supported, noncontacting magnetic field assembly that concentrates a strong magnetic field across an annular gap in which the coil fits (Fig. 3).[8] The linear range of these devices is about ± 2 mm. The lightest and most flexible electrical cables available were attached to the structure-borne coils and accelerometer, and they did not modify the structure's dynamics to a measurable degree.

Only one precedent in traveling wave experiments is known to the authors for the type of force actuators and velocity sensors used in this study. In 1954, Jones[3] reported a successful experiment on beams in which unit step forces were applied and response velocities were measured by means of magnet-coil devices similar to those described here.

All tests were conducted with a Synergistic Technology Inc. STI-11/23 16-channel data acquisition and analysis system running STI-VAMP Version 5A software. The system generated excitation signals and acquired and processed data signals.

Figure 7 shows the final support structure configuration. A framework of steel angles surrounding the aluminum grid is anchored to the cinderblock wall behind the grid and the thick concrete floor below. The magnetic field assemblies of the velocity sensors are clamped to this framework; mounting brackets for eight of the magnetic field assemblies and octagonal magnetic flux shields for another three are the light-colored objects directly behind the grid joints in Fig. 7.

The framework itself has natural frequencies as low as about 15 Hz. Tests showed that vibration of the framework could be detected by the velocity sensors and could corrupt the response data of the grid. Therefore, it was necessary to minimize excitation of the framework, which meant that the magnetic field assemblies of the force actuators should not be mounted on the framework. Hence, they were mounted on heavy instrument cabinets, which are in front of joints 1 and 4 in Fig. 7.

After all experimental refinements were effected, dynamic reciprocity tests were run to evaluate the adequacy and limitations of the experimental apparatus and procedure. Williams et al.[5] had previously conducted similar tests. Transient wave reciprocity between joints 1 and 4 of the aluminum grid was measured for SAS excitation frequencies of 30, 60, 120, and 240 Hz. Joint 1 was chosen in addition to joint 4 because it was easy to mount a second force actuator at joint 1.

Figure 8 shows some of the measured reciprocity data. Slightly different SAS force levels were imposed on joints 1 and 4. But the response was presumably linear, so velocities per unit force amplitude, $V_1(t)/\bar{F}_4$ and $V_4(t)/\bar{F}_1$, are directly comparable. Therefore, for each excitation frequency, these two relative velocity time series are plotted on the same graph of Fig. 8.

The upper graph of Fig. 8 shows that the responses for 120 Hz were nicely reciprocal. The two different time series are, for the most part, within a line width of each other. The small differences that can be detected are due to noise and limited measurement resolution. The responses for 30 and 60 Hz were comparably reciprocal.[16]

The lower graph of Fig. 8 shows that the 240-Hz response was much less reciprocal than those at lower frequencies. Differences in the synchronous components of response are especially noticeable. It seems unlikely that the laboratory structure itself was nonlinear, so the differences between the two measurements are probably due to diminished capability of the instrumentation at the higher frequency.

V. Transient Response Theory

The structure is assumed to be linear, with viscous inherent damping that does not couple the undamped normal modes of vibration. It is represented theoretically by an N-DOF finite-element model with matrix equation of motion

$$[m]\ddot{q}+[c]\dot{q}+[k]q=f \tag{1}$$

The $N\times N$ matrices $[m]$, $[c]$, and $[k]$ are mass, noncoupling inherent viscous damping, and stiffness matrices, respectively; $q(t)$ is the vector of all DOF, consisting of grid-point translations and rotations; and $f(t)$ is the vector of grid-point excitations.

For SAS point-force excitation with frequency Ω at DOF j, we have

$$f^T(t)=[0,\ldots,0,f_j(t),0,\ldots,0] \tag{2a}$$

where

$$\begin{aligned} f_j(t)&=0, && t<0\\ &=F_j\sin\Omega t, && t\geqq 0 \end{aligned} \tag{2b}$$

The structure is motionless before $t=0$, so the initial conditions are

$$q(0)=\mathbf{0} \text{ and } \dot{q}(0)=\mathbf{0} \tag{3}$$

The structural dynamics eigenproblem from Eq. (1) is

$$([k]-\omega_r^2[m])\Phi_r=\mathbf{0} \tag{4}$$

where ω_r and Φ_r are the natural frequency and mode shape vector, respectively, of the rth undamped mode of vibration. We solve Eq. (4) for all N modes and form the modal matrix $[\Phi]=[\Phi_1,\ldots,\Phi_N]$. Each mode shape vector is orthonormalized, $\Phi_r^T[m]\Phi_r=1$.

The standard modal transformation is

$$q=\sum_{r=1}^{N}\Phi_r\xi_r \tag{5}$$

where $\xi_r(t)$ is the rth modal coordinate. Substituting Eq. (5) into Eqs. (1) and (3), applying the standard orthogonality equations, and using Eq. (2) gives the following uncoupled initial-value problem for each modal coordinate $r=1,2,\ldots,N$:

$$\begin{aligned} &\ddot{\xi}_r+2\zeta_r\omega_r\dot{\xi}_r+\omega_r^2\xi_r=0, && t<0\\ &\qquad\qquad =\Phi_{jr}F_j\sin\Omega t, && t\geqq 0\\ &\xi_r(0)=0, \quad \dot{\xi}_r(0)=0 \end{aligned} \tag{6}$$

where ζ_r is the inherent viscous damping factor of the rth mode. The solution of Eq. (6) derived by elementary

methods is

$$\xi_r = C_{jr}\{(\omega_r^2-\Omega^2)\sin\Omega t - 2\zeta_r\omega_r\Omega\cos\Omega t + \Omega e^{-\zeta_r\omega_r t}[2\zeta_r\omega_r\cos\omega_{dr}t + \omega_{dr}^{-1}(2\zeta_r^2\omega_r^2+\Omega^2-\omega_r^2)\sin\omega_{dr}t]\} \quad (7)$$

where $C_{jr} = \Phi_{jr}F_j/[(\omega_r^2-\Omega^2)^2+(2\zeta_r\omega_r\Omega)^2]$ and $\omega_{dr} = \omega_r\sqrt{(1-\zeta_r^2)}$.

Since response is assumed to be linear, it is appropriate to compute any motion quantity as motion per unit force amplitude. Such relative motion quantities simplify comparison of theoretical and experimental results in the next section. As is explained in Sec. IV, it is most appropriate to compute response velocity rather than displacement or acceleration. From Eqs. (5) and (7) then, the relative velocity of DOF i due to SAS excitation at DOF j is

$$\frac{\dot{q}_i}{F_j} = \sum_{r=1}^{N}\Phi_{ir}\left(\frac{\dot{\xi}_r}{F_j}\right) \quad (8)$$

Note that the contribution of all modes of the finite-element model are summed in Eq. (8). Hence, this solution is fully equivalent to direct integration of the model's complete set of differential equations of motion, Eq. (1).

VI. Comparison of Experimental and Theoretical Transient Response Results

Values of modal damping factors ζ_r for low-frequency modes of the laboratory structure have been measured previously.[10] These values were 0.04 for mode 1, 0.03 for modes 2 and 3, 0.01 for mode 4, 0.006-0.002 for modes 5-15, and 0.0011-0.0015 for modes 16-22. These values and the estimate 0.001 for all $r>22$ were used in preliminary numerical evaluations of Eq. (8) at SAS excitation frequencies of 30 and 240 Hz. For comparison, Eq. (8) was evaluated for the same frequencies and zero damping in all 127 modes.

The comparison demonstrated that the damping factors used have very little influence on the transient response over the short times considered in this study. The greatest differences between damped and undamped responses were less than the differences evident on the 120-Hz reciprocity graph of Fig. 8. Because damping has such little effect and modal damping factors are approximate at best, the damping factors of all modes were set to zero for the theoretical calculations presented.

Figures 9 and 10 are representative experimental and corresponding theoretical transient responses for SAS excitation frequencies 30 and 90 Hz. The selection of these particular frequencies was based on the experimental-theoretical modal density comparison of Fig. 4. The theoretical modal density prediction is good at 30 Hz but inaccurate at 90 Hz. References 16 and 17 include the same type of figures for the other SAS excitation frequencies evaluated: 15, 45, 60, 120, 150, and 240 Hz.

SAS force excitation was applied at joint 4. Relative velocities at joints 4, 3, 8, 1, 5, 10, and 9 are plotted, respectively, from top to bottom in Figs. 9 and 10. These joints and this ordering were selected to help illustrate the progression of the wavefront leftward and upward from joint 4.

The agreement between experiment and theory is generally good in Fig. 9 for 30-Hz SAS excitation. The wavefront arrival times are the same, and all responses are very similar for the first 0.15 s. The agreement is less satisfactory for $t>0.2$ s, especially for the magnitudes of response at joints 3, 5, and 9.

The ability of the theory to predict the measured response seems to depend partly upon whether the response consists primarily of traveling or of standing waves. Consider, for example, the response at joint 9 for the 30-Hz case. The theory accurately predicts the traveling wave arrival time (about $t=0.07$ s) and the response for about 0.2 s after arrival, but for $t>0.3$ s, the predicted response differs markedly in magnitude from the measured response.

Joint 9 is close to the steel top beam assembly and to a nominally rigid support boundary (see Fig. 1), so wave reflection from these stiff members near joint 9 obviously begins at about $t=0.1$ s. After that time, superposition of waves traveling outward from joint 4 and waves reflecting from all boundaries appears to convert the net response

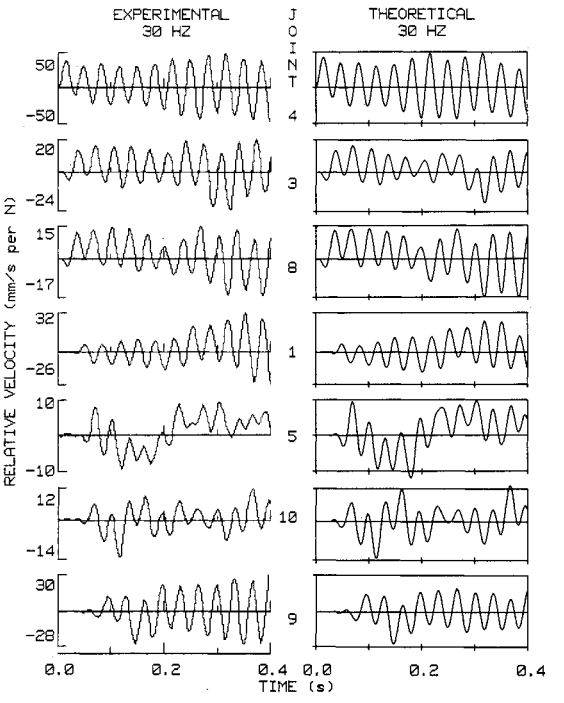

Fig. 9 Response to 30-Hz SAS force at joint 4 beginning at $t=0$ s. The force amplitude in the experiment was 0.337 N (0.0757 lb).

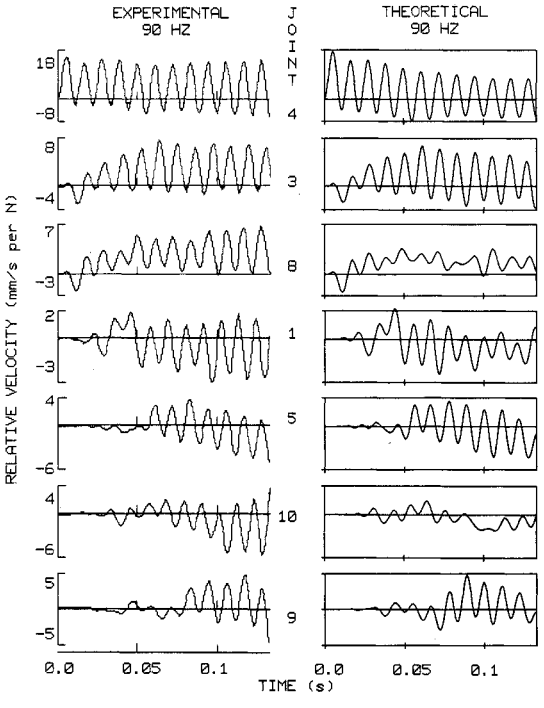

Fig. 10 Response to 90-Hz SAS force at joint 4 beginning at $t=0$ s. The force amplitude in the experiment was 0.840 N (0.189 lb).

gradually into standing waves dominated by one or a few modes whose natural frequencies are close to the excitation frequency.

Predicted standing wave response can be no more accurate than the theoretical shapes of the dominant modes. However, it is unlikely that the theoretical shapes of high-frequency modes are accurate throughout the aluminum grid, even for modes around 30 Hz, where the mode count accuracy is good. High-frequency mode shape inaccuracy is especially likely near the bolted joints, because concentrated joint masses tend to produce displacement nodal regions. Hence, the prediction error for $t>0.3$ s in the joint 9 response of Fig. 9 is probably due to mode shape inaccuracy.

The accuracy of theoretical prediction for the 90-Hz case of Fig. 10 is not as good, in general, as that for the 30-Hz case. The measured driving-point response of joint 4 has substantially more positive bias than does the predicted response. At higher frequencies, this inaccuracy and overestimation of peak-to-peak oscillatory driving-point magnitude become progressively worse.[16,17] As in the 30-Hz case, theoretical prediction accuracy is good for the form and magnitude of initial waves at joints away from the driving point and generally not so good at later times when standing waves develop.

Close examination of responses away from the driving point in the 90-Hz data reveals a prediction error not detectable in the 30-Hz data: the computed traveling wave speed is higher than the observed speed. This is manifested by arrival of the first few wave peaks in the theoretical plots on the order of 1 ms earlier than their counterparts in the experimental plots. This inaccuracy is detectable in the data for all SAS excitation frequencies above 30 Hz.[16,17] The degree of wave speed overestimation seems to increase progressively with frequency, but the measured data are not sufficiently precise to permit a firm conclusion. Wave speed inaccuracy is probably a consequence of the finite-element model's greater stiffness, in general, than that of the actual structure.

VII. Concluding Remarks

An experimental procedure was developed for generating and measuring transient waves in a two-dimensional laboratory structure. Representative measurements are compared herein with theoretical predictions based on a refined finite-element model of the structure.

Suddenly applied sinusoidal (SAS) point-force excitation was used. This permitted evaluation of the finite-element model's ability to predict transient response for eight SAS frequencies from 15–240 Hz. Comparison of theoretical and experimental results suggests that the finite-element model does a good job, for the most part, of predicting the first phase of transient response, which consists primarily of traveling waves. However, the traveling wave speed is overestimated for all SAS frequencies above 30 Hz. The model predicts less accurately the second phase of response, after waves reflected off boundaries become significant. Moreover, the prediction accuracy deteriorates as the SAS frequency increases. These observations strongly suggest that the second phase of response consists primarily of standing waves dominated by a small number of modes, and that the inaccuracy in prediction is due to inaccuracy of theoretical mode shapes.

A reviewer of this paper has asked the question, "Why does the finite-element model, despite having inaccurate modal parameters for the majority of modes, give reasonably good predictions of initial traveling wave response?" That question is certainly worthy of careful study, but a detailed examination is beyond the scope of this paper. However, the authors feel that two general features of the theoretical model are instrumental to its success. First, its modal density (Fig. 4) is accurate for frequencies below 57 Hz and is probably at least a fair approximation up to much higher frequencies. Second, the complete set of eigenvectors (mode shapes) of the theoretical model, although not those of the actual structure, nevertheless probably do a good job of spanning the vector space of the actual response.

The laboratory structure's relatively small size permitted only brief periods for waves to travel away from the point of excitation before reflecting off boundaries. It is doubtful that steady-state, synchronous traveling waves had time to develop during these periods. A more complete study of wave propagation without the complication of boundary reflection would require a comparably flexible structure extending over a very much larger area. With such a structure and the use of strain gages in addition to the instrumentation and techniques described herein, it might be possible to distinguish synchronous waves from precursor waves and to infer group and phase velocities.

Acknowledgments

This work was sponsored by AFOSR Contract F49620-85-C-0024, Dr. A. K. Amos, Structural Mechanics Program Manager. The system for data acquisition and analysis was purchased with NSF Grant CME-8014059.

References

[1]von Flotow, A. H., "Disturbance Propagation in Structural Networks," *Journal of Sound and Vibration*, Vol. 106, No. 3, May 8, 1986, pp. 433–450.

[2]Mead, D. J., "A New Method of Analyzing Wave Propagation in Periodic Structures; Applications to Periodic Timoshenko Beams and Stiffened Plates," *Journal of Sound and Vibration*, Vol. 104, Jan. 8, 1986, pp. 9–27.

[3]Jones, R. P. N., "The Wave Method for Solving Flexural Vibration Problems," *Journal of Applied Mechanics*, Vol. 21, No. 1, 1954, pp. 75–80.

[4]Roy, A. K. and Plunkett, R., "Dispersive Bending Waves in Uniform Bars," *Experimental Mechanics*, Vol. 25, No. 3, Sept. 1985, pp. 308–311.

[5]Williams, J. H. Jr., Zhang, J. J., and Lee, S. S., "Wave Propagation Measurements on Two-Dimensional Lattice," NTIS Accession AD-A166207, Sept. 1985.

[6]Williams, J. H., Jr., Ou, H. L., and Lee, S. S., "Wave Measurements on Truss Model," NTIS Accession AD-A162433, Sept. 1985.

[7]Bozich, W. F., *Wave Propagation in Simple Nonhomogeneous Systems with a Transition Point*, Ph.D. Dissertation, Dept. of Aeronautics and Astronautics, Stanford Univ., CA, 1971.

[8]Hallauer, W. L. Jr., Skidmore, G. R., and Gehling, R. N., "Modal-Space Active Damping of a Plane Grid: Experiment and Theory," *Journal of Guidance, Control, and Dynamics*, Vol. 8, No. 3, May/June 1985, pp. 366–373.

[9]von Flotow, A. H., "Low Authority Control Synthesis for Large Spacecraft Structures, Using Disturbance Propagation Concepts," *Proceedings of the AIAA/ASME/ASCE/AHS 26th Structures, Structural Dynamics and Materials Conference*, Part 2, April 1985, pp. 152–160.

[10]Skidmore, G. R. and Hallauer, W. L. Jr., "Experimental-Theoretical Study of Active Damping with Dual Sensors and Actuators," *Proceedings of the AIAA Guidance, Navigation, and Control Conference*, Aug. 1985, pp. 433–442.

[11]Craig, R. R. Jr., *Structural Dynamics, An Introduction to Computer Methods*, Wiley, New York, 1981, pp. 383–389.

[12]Argyris, J. H., Hilpert, O., Malejannakis, G. A., and Scharpf, D. W., "On the Geometrical Stiffness of a Beam in Space—A Consistent V.W. Approach," *Computer Methods in Applied Mechanics and Engineering*, Vol. 20, 1979, pp. 105–131.

[13]Przemieniecki, J. S., *Theory of Matrix Structural Analysis*, McGraw-Hill, New York, 1968, pp. 79–80, 295–297.

[14]Lyon, R. H., *Statistical Energy Analysis of Dynamical Systems: Theory and Applications*, The MIT Press, MA, 1975, pp. 278–279.

[15]Hallauer, W. L. Jr., "Transient Waves in a Beam Excited by Sinusoidal Edge Shear Force," *Journal of Applied Mechanics*, Vol. 54, June 1987, pp. 468–470.

[16]Hallauer, W. L. Jr. and Trivedi, D. J., "An Experimental Study of Transient Waves in a Plane Grid Structure, *Proceedings of the AIAA Dynamics Specialists Conference*, Part 2B, April 1987, pp. 888–899.

[17]Hallauer, W. L. Jr., "Experimental Study of Active Vibration Control," Final Rept., AFOSR Contract F49620-85-C-0024, Aug. 1987.